DOI:
10.1021/acsami.8b00370

Document Version
Peer reviewed version

Multi-Scale Engineered Si/SiO_x Nanocomposite Electrodes for Lithium Ion Batteries Using Layer-by-Layer Spray Deposition

Chun Huang,[a] Ayoung Kim,[b] Dong Jae Chung,[b] Eunjun Park,[b] Neil P. Young,[a] Kerstin Jurkschat,[a] Hansu Kim,[b,*] Patrick S. Grant,[a,*]

[a]*Department of Materials, University of Oxford, Parks Road, Oxford, OX1 3PH, United Kingdom*

[b]*Department of Energy Engineering, Hanyang University, 222 Wangsimni-ro, Seongdong-gu, Seoul, 04763, South Korea*

Corresponding Author Information

*E-mail: khansu@hanyang.ac.kr; patrick.grant@materials.ox.ac.uk

Keywords

Lithium ion battery, Si/SiO_x nanocomposite, electrode architecture, layer-by-layer, scalable spray deposition

Abstract

Si-based high capacity materials have gained much attention as an alternative to graphite in Li ion battery anodes. Although Si additions to graphite anodes are now commercialised, the fraction of Si that can be usefully exploited is restricted due to its poor cyclability arising from the large volume changes during charge/discharge. Si/SiO_x nanocomposites have also shown promising behaviour, such as better capacity retention than Si alone because the amorphous SiO_x helps to accommodate the volume changes of the Si. Here we demonstrate a new electrode architecture for further advancing the performance of Si/SiO_x nanocomposite anodes using a scalable layer-by-layer atomisation spray deposition technique. We show that particulate C interlayers between the current collector and the Si/SiO_x layer, and between the separator and the Si/SiO_x layer, improved electrical contact and reduced irreversible pulverisation of the Si/SiO_x significantly. Overall, the multi-scale approach based on micro-structuring at the electrode level combined with nano-engineering at the material level improved the capacity, rate capability and cycling stability compared with an anode comprising a random mixture of the same materials.

1. Introduction

Rechargeable Li-based batteries with high energy densities of typically 260-310 Wh kg^{-1} have been pursued intensively to meet the demands of high capacity, high power, reduced cost and extended lifetime for portable electronics and electric transportation applications.[1] Graphite is currently used as the active anode material in commercial Li ion batteries (LIBs) because it is comparatively cheap, acceptably robust in service and easy to process into large electrode areas by slurry coating, but has a limited theoretical capacity of 372 mAh g^{-1} for Li ion intercalation.[2] Si has a much higher and attractive theoretical capacity of 3579 mAh g^{-1} as an LIB anode, through an alloying mechanism with Li that forms crystalline $Li_{15}Si_4$ with the potential to significantly increase overall battery energy densities.[3] However, Si expands up to 400% by volume on full Li insertion, with a similar contraction on Li extraction,[4] which causes the well-known Si pulverisation and fracture, resulting in a loss of electrical

contact in the electrode, ongoing surface reactions to form solid electrolyte interface (SEI) with a loss of Li,[5] and even macro-scale electrode cracking and delamination from the current collector.[6] SiO_x based anode materials show a smaller and potentially easier to accommodate volume change of up to 160% upon Li insertion, and a corresponding lower theoretical capacity of 3172 mAh g^{-1}.[7-14]

To address the shortcomings of Si as an anode, a wide range of Si and/or SiO_x nanomaterial design concepts have been developed, including one-dimensional Si nanowires,[15] hollow nanoparticles,[16] nanotubes,[17] Si-C nanocomposites,[18-19] double-walled Si-SiO_2 hollow tubes [20] and Si-C "pomegranate" structures.[21] Common to all the nano-scale approaches is the idea that strain in such nanostructures can be relaxed without mechanical fracture because induced defects, such as dislocations, can readily run out to the free surface so that significant plastic deformation and macro-scale failure are avoided.[22] However, the intrinsic high surface area of nanostructures promotes SEI and other parasitic reactions with the electrolyte that, as previously described, consume Li ions and give unstable and short cycle lifetimes. Although C coatings have been added on individual Si-based nanoparticles to prevent direct contact between the Si-based nanoparticles and the electrolyte,[23-25] if the ratio between the C coating thickness and the Si-based nanoparticle size is not controlled carefully, the stiff C coatings may fracture when the Si-based nanoparticles expand,[26] and the cracks in the C coatings are prone to penetrate into the Si-based nanoparticles and induce fracture of the nanoparticles.[27] In general terms, nanostructures also usually reduce electrode volumetric capacities (due to low electrode tap density) that is a critical performance parameter for commercial applications.[28] Additionally, many of the studies have focused on thin-film electrodes (140-200 nm) made by fabrication techniques such as magnetron sputtering that are difficult to scale up.[29]

Most commercial LIB electrodes are made by a slurry coating process (doctor-blade coating of a mixed slurry onto a current collector foil followed by drying) that results in an electrode microstructure comprising a random mixture of active, binder and electrically conducting materials, along with interconnected pores.[30] However, both computer simulations[31] and experimental results[32] have shown that electrolyte concentration is not homogeneous through the electrode thickness of these random electrode structures due to electrolyte ions mass transfer resistance, leading to an electrolyte

concentration gradient where local Li ion concentration is the highest nearest the separator and lowest nearest the current collector.[33, 34] Hence, accelerated performance degradation occurs especially at the interface between the electrode and separator,[27] and experimental results have shown that a porosity graded electrode structure reduced capacity fade by ~8.3% in full cells and ~5.3% in half cells.[32] Because of the convenience of slurry coating, but also accepting its inherent lack of microstructural control, there have been few investigations of how more controlled electrode structures might be used to further facilitate improved cycling or other metrics of potentially high-performing electrode materials, including Si or SiO_x. Our previous work concerning a two-layer TiO_2-based anode structure in which each layer comprised a different TiO_2 morphology, showed how the two-layer electrode volumetric capacity was increased by 72% at a relatively fast (dis)charge rate of 2 C compared with a standard anode containing a conventional, randomly mixed microstructure of the same materials.[35]

Here, we take the concept of the layered electrode further and combine a micro-scale, layered electrode design with a nano-scale Si/SiO_x composite material as a way to accommodate a high capacity but high expansion Si-based anode for LIBs. We have chosen Si/SiO_x as a model high capacity material to demonstrate the effect of changes in electrode micro-architecture on the overall electrochemical performance. A nanocomposite of Si/SiO_x comprising 7-15 nm Si nanocrystals embedded in 140-250 nm amorphous SiO_x nanospheres (Figure 1(a)) was synthesised by a cost effective sol-gel method.[36] The intention was that the comparatively mechanically robust SiO_x matrix phase should act as a mechanical buffer to accommodate the volume changes of Si during cycling at the nano-scale. Then, to accommodate further the Si/SiO_x volume changes at a higher length scale and to improve electrical contact, distinct Si/SiO_x nanocomposite layers were interleaved with either one or two C black nanoparticle layers (Figure 1(b)). We show that the discrete C layers effectively buffered the volume expansion of the Si/SiO_x layer, and improved electrical interfacial contact and cycling stability when compared with a conventional random mixture of the identical materials. We propose that this facile layering of the electrode structure may find wider applicability in other high-capacity alloy-type electrode materials that similarly suffer from large volume changes during cycling, and in other energy

systems such as Li-air, Li-S and Na-ion batteries where electrode-scale microstructural design has yet to be explored.

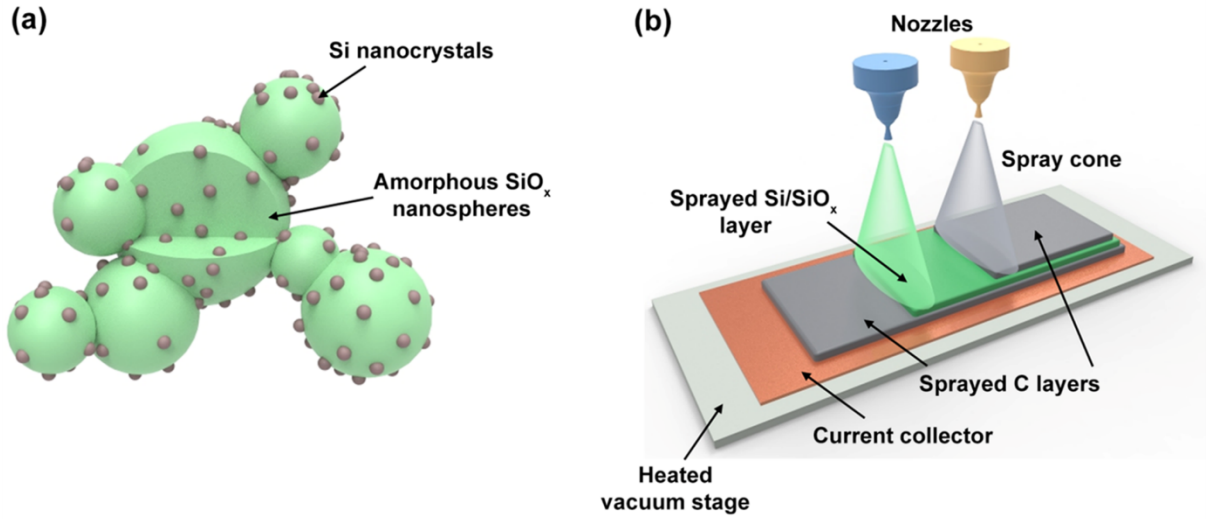

Figure 1. Schematics of (a) the Si/SiO_x nanocomposite arrangement consisting of 7-15 nm Si nanocrystals embedded in 140-250 nm amorphous SiO_x nanospheres; and (b) layer-by-layer atomisation spray deposition to make the various layered anode structures.

2. Experimental

2.1 Material preparation

The Si/SiO_x composite was synthesised using a sol-gel reaction of triethoxysilane $(C_2H_5O)_3SiH$ to form hydrogen silsesquioxane $HSiO_{1.5}$ nanospheres, followed by thermal treatment, as reported previously.[36] First, 10 ml of $(C_2H_5O)_3SiH$ [Sigma Aldrich, 99.8%] was slowly dropped into a 0.1 M HCl solution (500 ml) under continuous stirring at 800 rpm. The solution was filtered and washed with deionised water repeatedly. The precipitates of $HSiO_{1.5}$ were collected and dried in an oven at 100 ^oC to eliminate residual moisture. After fine grinding, the $HSiO_{1.5}$ powders were heated at 900 ^oC at a heating rate of 20 ^oC min^{-1} for 1 hr under a 4% H_2/Ar atmosphere at a flow rate of 0.5 l min^{-1}. The thermal decomposition of $HSiO_{1.5}$ reduced $HSiO_{1.5}$ to Si nanocrystals embedded in a SiO_x matrix,[31] as shown by detailed characterisation in the following section. Changing the heating temperature and duration will change the size of the Si nanocrystals as reported previously.[36-38]

2.2 Electrode fabrication

We have previously reported the atomisation spray processing developed for electrodes in our group,[39-40] which is shown schematically in Figure 1(b). Briefly, two suspensions were prepared: "A" - the C black nanoparticle layer, and "B" - the Si/SiO_x nanocomposite layer. Suspension "A" contained C black (Super-P, Alfa Aesar, 90 wt%) and a binder of poly(vinylidene fluoride) (PVDF, Sigma Aldrich, 10 wt%). Suspension "B" contained Si/SiO_x (80 wt%), C black (10 wt%) and PVDF (10 wt%); both suspensions utilised *n*-methyl-2-pyrrolidone (NMP) as the fugitive carrier liquid.[41]

During electrode fabrication, suspensions "A" and "B" could be fed to two atomisation nozzles and sprayed sequentially in a continuous process with no break between the formation of discrete layers. The suspensions were atomised into fine droplets by compressed air and deposited onto a Cu foil current collector, maintained at 200 ^{o}C throughout fabrication on a heated vacuum stage. The NMP component evaporated continuously on the heated vacuum stage as the layers were deposited successively and there was no build-up of liquid on the current collector as the electrode was formed. The nozzles moved in a pre-programmed zig-zag pattern along *x* and *y* directions to spray an electrode up to 20 cm x 20 cm. The production speed was ~7 μm cm^{-2} per nozzle.

To investigate energy storage benefits of the layered electrode structures, four types of anode were made: (a) a layer of C black on the Cu current collector and then a layer of Si/SiO_x, termed [Bottom C]; (b) a layer of Si/SiO_x on the Cu current collector and then a layer of C black [Top C]; (c) a layer of C black on the Cu current collector, then a layer of Si/SiO_x and finally another layer of C black [Sandwich]; and (d) a conventional, random mix of the same materials [Blended]. All of the electrodes had a similar final mass loading, or electrode "weight" of 1.1 mg cm^{-2} ± 5%, and similar to other Si-based electrodes from the literature.[36] The mass ratio of Si/SiO_x : C nanoparticles was approximately 1.5 in the electrodes, although there were likely some differences estimated at 10-15% among different electrode structures, as it was not always possible to keep more precise control of the relative thickness of discrete layers. For a fair comparison between the different structured electrodes, the total electrode mass (Si/SiO_x + C black + binder) was used in all calculations of the gravimetric capacities unless otherwise stated.

2.3 Characterisation

X-ray diffraction (XRD) data was collected from the Si/SiO_x powders using an Empyrean diffractometer (PANalytical) equipped with monochromated Cu Kα radiation (λ = 1.54056 Å). The morphology of the Si/SiO_x powders and the electrodes were characterised using a field emission scanning electron microscopy (SEM, JEOL JSM-7000F and Zeiss Merlin Gemini 2). Cross sections of the electrodes were prepared using a cross-section polisher (CP, JEOL SM-09010). The size, structure and crystallinity of individual Si/SiO_x particles were characterised using transmission electron microscopy (TEM, JEOL 3000F). Si/SiO_x powders were first embedded in resin (Agar 100), TEM samples were then prepared from cutting the hardened resin containing the Si/SiO_x powders into thin slices using an ultramicrotome (LKB Bromma Ultratome Nova). X-ray photoelectron spectroscopy (XPS) was performed in an ion pumped Thermo Scientific K-Alpha 128-channel detecting analyser equipped with an Al Kα X-ray source. The X-ray beam irradiated the surface of the four types of as-sprayed electrodes, and provided an X-ray spot size of 800 x 800 μm^2. Wide scans of the surface of the samples were performed at 100 eV, and detailed scans were performed at 20 eV. Detailed scans were collected at three different points on each sample to obtain representative data. The quantification of the fitted peaks was carried out using Avantage Version V5.952 software. Prior to peak fitting, the background contributions were subtracted using a Shirley function. All of the XPS detailed scans were first calibrated based on C_{1s} photoemission peak at 284 eV for a fair comparison among different samples.

The electrochemical properties of the electrodes were characterised using coin type half-cells (CR2032). The cells were carefully assembled in an Ar-filled glovebox using Li metal as a counter electrode and polyethylene (PE) membrane as a separator. The electrolyte was 1 M $LiPF_6$ dissolved in a mixed solvent of ethylene carbonate (EC) and ethyl methyl carbonate (EMC) (3:7, v/v) with 2.0 % fluoroethylene carbonate (FEC) (Panax Etec). The cells were galvanostatically charged and discharged in the voltage range of 0.005−2.0 V (vs Li/Li^+) at different current densities at room temperature. Electrochemical impedance spectroscopy (EIS) measurements were collected using an impedance analysing potentiostat (VSP-300, BioLogic) with an AC amplitude of 10 mV and a frequency range of 10 mHz and 1 MHz

for the four types of electrode in the conditions of as-sprayed, after first lithiation, after one lithiation and delithiation cycle, and after the 5th cycle lithiation and delithiation. For *ex-situ* SEM observations of the cycled electrodes, the electrodes were carefully disassembled from the cells and then rinsed with dimethyl carbonate (DMC) in an Ar-filled glovebox to remove any residual electrolyte.

3. Results and discussion

3.1 Si/SiO$_x$

Figure 2(a) is an SEM image of the Si/SiO$_x$ nanocomposite powders showing approximately spherical particles with diameters sizes ranging between 140 nm and 250 nm. Figure 2(b) shows a magnified SEM image of the individual Si/SiO$_x$ particles containing crystalline spheres of 7-15 nm embedded in the larger spheres that lacked any distinct crystallographic features. Figure 2(c) shows an XRD pattern of the synthesised Si/SiO$_x$ powders exhibiting a broad Bragg peak at 21° typical for very fine-scale crystalline Si embedded in amorphous SiO$_x$.[10, 42] Figure 2(d) shows a TEM image of an individual Si/SiO$_x$ nanosphere with a diameter of ~230 nm, and darker nanoparticles of relatively uniform sizes embedded in the nanosphere. Figure 2(e) shows a magnified region of Figure 2(d), showing the crystallinity of the embedded Si nanoparticles and their sizes in the range of 7-15 nm, and the amorphous nature of the surrounding SiO$_x$ phase. Figure 2(f) shows a further magnified TEM image, confirming that the *d* spacing of the Si nanocrystals was ~3.1 Å, in agreement with crystalline Si (111).[31]

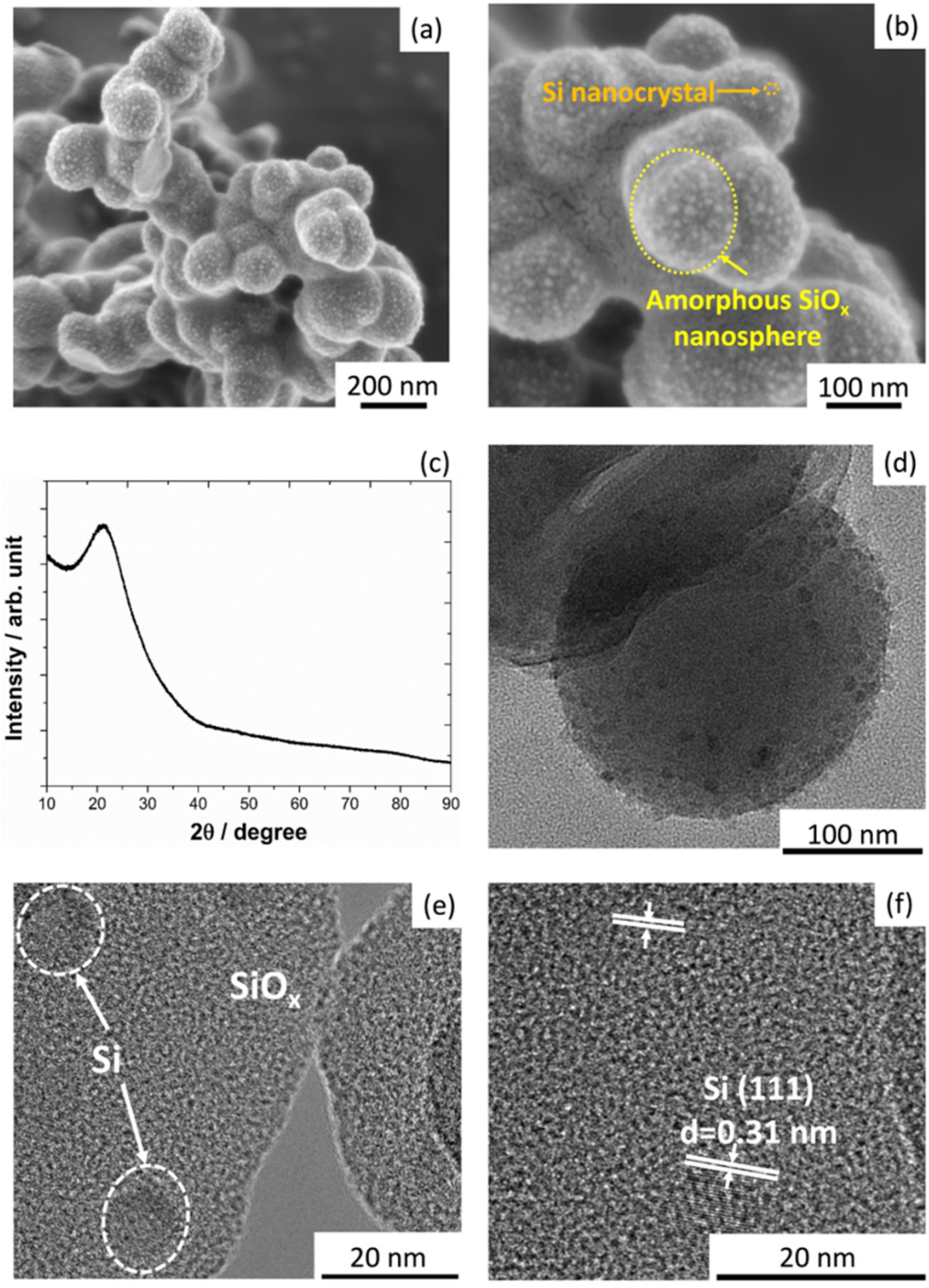

Figure 2. (a) SEM image of the laboratory synthesised Si/SiO_x powders, which is magnified in (b). (c) XRD pattern of the Si/SiO_x powders. (d) TEM image of an individual Si/SiO_x particle. (e) A magnified image of the Si/SiO_x particle showing crystalline Si nanoparticles embedded in the amorphous SiO_x phase. (f) A further magnified image showing *d* spacing of the crystalline Si.

Figure 3 shows the XPS detailed scans of the Si_{2p} spectrum for the four types of as-sprayed electrode. A peak at 99.7 eV corresponding to elemental Si was present in all of the samples,[8] indicative of the presence of Si nanocrystals, in agreement with the TEM results in Figure 2. The other two dominant peaks were at 102.7 and 103.8 eV, corresponding to Si^{3+} and Si^{4+} respectively,[8] and indicative of silicon suboxides SiO_x. The ratio between SiO_x and Si was estimated from the ratio between the total peak area of Si^{3+} and Si^{4+} and the Si peak area. This ratio was relatively constant among all samples at an average of 2.9, demonstrating an approximately constant fraction of Si.

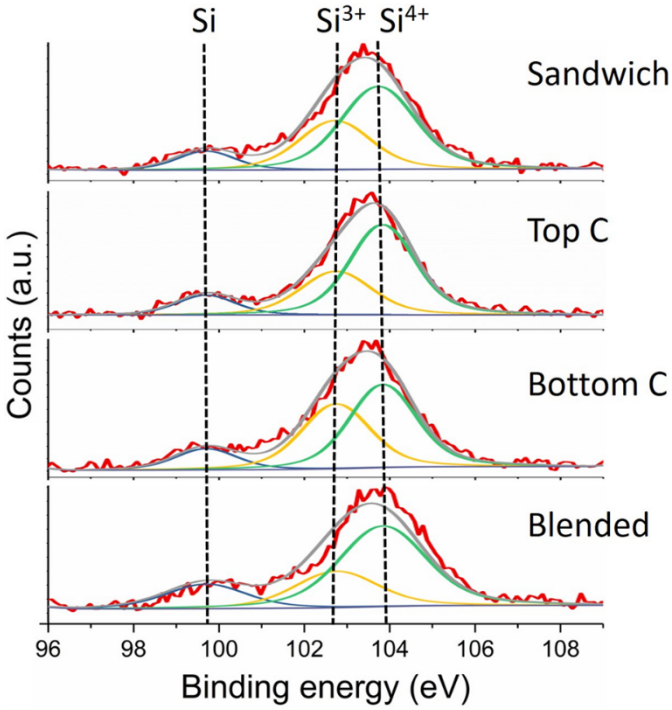

Figure 3. XPS detailed scans of Si_{2p} spectrum for the four types of as-sprayed electrode.

3.2 Electrode structure

Figure 4 shows cross-sectional SEM images of the as-sprayed electrodes, across a relatively large area along with the corresponding energy dispersive X-ray spectroscopy (EDS) elemental maps for C, Si and O, for the four types of electrode. All the electrodes showed porous structure with an average electrode thickness of 11.4 µm. Figure 4 shows how the layer-by-layer spray deposition placed the C and Si/SiO_x nanoparticles in different layers, albeit with some inter-mixing at the interface between the

layers, as the layers were not perfectly flat, and some transitory re-suspension of the material at the free layer surface was expected as the next layer of droplets deposited and the NMP evaporated.

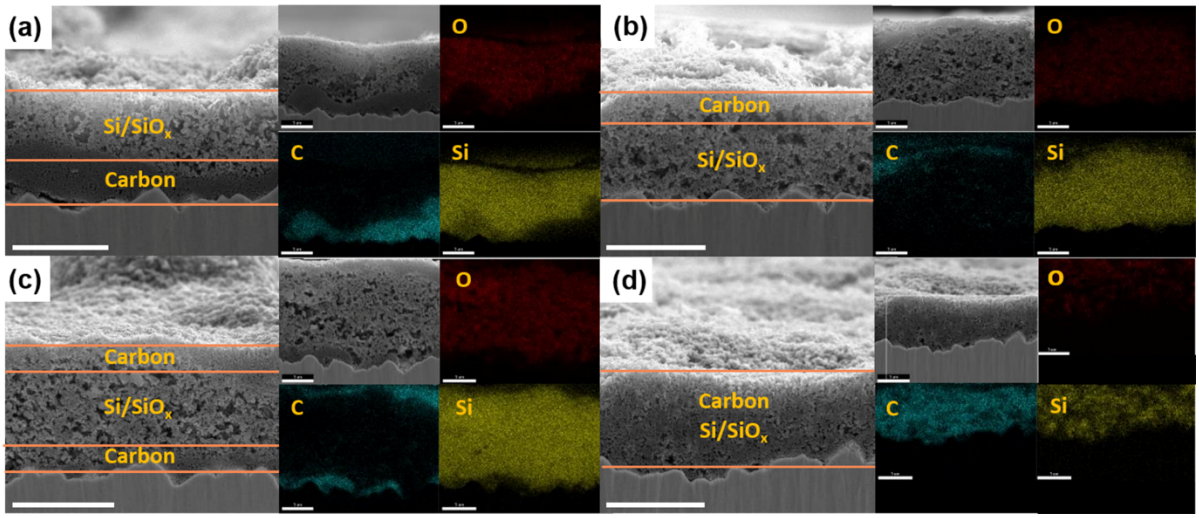

Figure 4. Cross-sectional SEM images of the as-sprayed electrodes and the corresponding EDS C, Si and O elemental maps for (a) [Bottom C] electrode; (b) [Top C] electrode; (c) [Sandwich] electrode; and (d) [Blended] electrode. Scale bars in the cross-sectional SEM images are 10 µm, scale bars in the EDS images are 1 µm.

3.3 Electrochemical performance

Figure 5(a) shows the galvanostatic voltage profiles of the four types of electrode at a rate of 50 mAg^{-1} for the first cycle. All of the electrodes exhibited a voltage plateau at approximately 0.2 V *vs* Li/Li^+ during lithiation and a sloped plateau at 0.25-0.55 V *vs* Li/Li^+ during delithiation.[43] In more detail, Li ion extraction from the Li-Si phase occurs at ~0.52 V *vs* Li/Li^+, while Li ion extraction from lithiated SiO_x occurs at ~0.3 V *vs* Li/Li^+;[44] the sloped plateaux in the range 0.25-0.55 V indicated that both Si and SiO_x phases in the nanocomposite contributed to electrochemical energy storage reaction involving Li ions.

The reversible capacities were estimated at 511, 493, 348 and 331 mAh g^{-1} for the [Sandwich], [Bottom C], [Top C] and [Blended] electrodes respectively, where the total electrode mass (Si/SiO_x + C black + binder) was used to estimate the gravimetric capacities. For comparison, based on the mass of the Si/SiO_x active material only, the estimated capacities were 852, 822, 580 and 552 mAh g^{-1} for the [Sandwich], [Bottom C], [Top C] and [Blended] electrodes, respectively. The reversible capacities of

the [Sandwich] and [Bottom C] electrodes at a relatively low current density were similar to each other and higher than those of the [Top C] and [Blended] electrodes. The capacity of the [Sandwich] electrode with respect to the mass of Si/SiO_x was higher than 438 mAh g^{-1} for an anode of ultra-fine SiO_x nanoparticles,[45] 650 mAh g^{-1} for an anode of SiO_x nanocomposite [46] and 645 mAh g^{-1} for an anode of blocky SiO_x/C with graphite-like structure,[47] but lower than ≥ 1000 mAh g^{-1} for other Si/SiO_x reported in [6-9, 36, 48-51], noting that the Si/SiO_x morphologies and the ratios of Si to SiO_x vary.[52]

Figure 5(b) shows the Coulombic efficiency of the four types of electrode with respect to cycling, and Figure 5(c) shows the magnified Coulombic efficiency of the four types of electrode at the initial 5 cycles. The Coulombic efficiency was calculated by dividing the delithiation capacity by the lithiation capacity at each cycle. The average initial Coulombic efficiency (ICE) at the first cycle was 39% for the four types of sprayed electrode, similar to 39.8% of ICE for a Si/SiO_x anode[53] and higher than 35.7% for a SiO/carbon nanofibers anode.[54] SiO_x normally exhibits a low ICE due to the formation of Li_2O, Li silicates and SEI from the first cycle,[29, 55] The Coulombic efficiency of all sprayed electrodes increased to more than 98% after the initial 5 cycles, similar to another high Coulombic efficiency SiO_x/C-based anode.[47] The Coulombic efficiency of all sprayed electrodes further increased to more than 99% after 100 cycles, higher than 87.9% after 100 cycles for an anode of $Si/SiO_x/C$ composite made via high-speed spray pyrolysis,[56] showing that electrochemical reaction of all of the sprayed electrodes were largely reversible, irrespective of the microstructure.

Figure 5(d) shows the reversible capacities of the four types of electrode at different current densities. The capacity of the [Sandwich] electrode with respect to the total electrode mass was the highest (511 to 429 mAh g^{-1}) at 50 to 250 mA g^{-1}, and the capacity of the [Bottom C] electrode was the highest at the highest rate of 2500 mA g^{-1}. The capacity retention of the [Bottom C] electrode was 85% from 100 mA g^{-1} to 1000 mA g^{-1}, much higher than the capacity retention of other electrodes containing $Si/SiO_x/C$ composites from the literature (*e.g.* 64% [57]).

Figure 5(d) also shows the reversible capacities of the four types of electrode at 50 mA g^{-1} from the 30^{th} to the 100^{th} cycle. The capacity of the [Blended], [Bottom C] and [Sandwich] electrodes decreased by

45%, 38% and 29% respectively, similar to other electrodes containing Si/SiO_x/C composites after 100 cycles from the literature.[58-59] Interestingly, the capacity of the [Top C] electrode increased by 11% from the first to the 100th cycle, even after varying the current density, showing excellent capacity stability, which was further investigated by EIS.

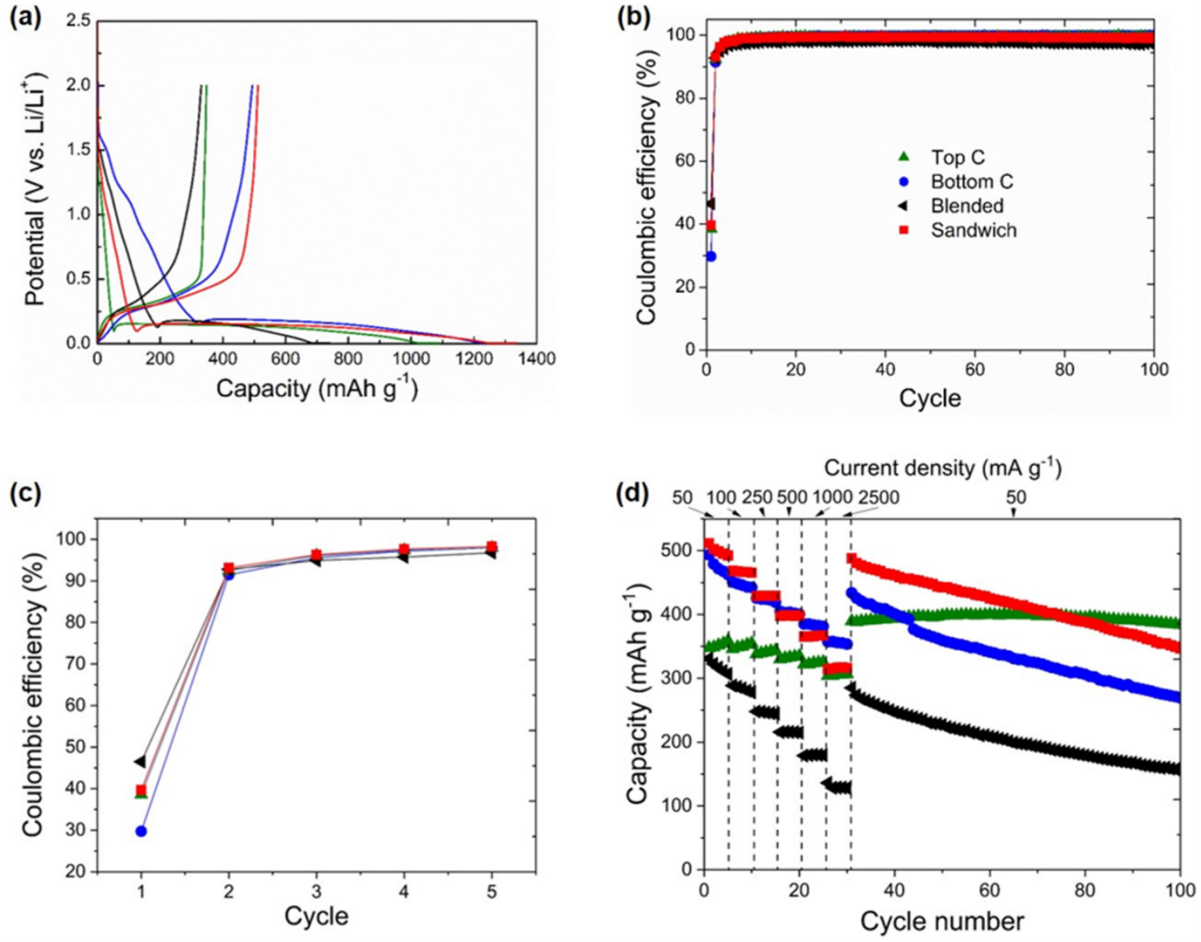

Figure 5. Electrochemical performance of the four types of electrode: (a) lithiation and delithiation profiles at 50 mA g^{-1} at the first cycle; (b) Coulombic efficiency; (c) magnified Coulombic efficiency data at the initial 5 cycles; and (d) rate capability and stability.

Figure 6(a) shows a Nyquist plot of the four types of as-sprayed electrode, consisting of a semi-circle at high frequency and a linear section at low frequency, similar to other pristine Si-based anodes.[60] The intercept between the Nyquist plot and the real *Z* axis represents electrolyte resistance (R_s) and was 0.7 – 3.5 Ω cm^2 for the four types of electrode. The diameter of the semi-circle at high frequency represents

charge transfer resistance (R_{CT}) which includes the interfacial resistance between the current collector and the electrode.[61] Figure 6(a) shows that R_{CT} of the [Sandwich] and [Bottom C] electrodes was lower than R_{CT} of the [Top C] and [Blended] electrodes.

Figure 6(b) shows a Nyquist plot of the four types of electrode after lithiation, with an additional semi-circle at median frequency and deviation of slope in the linear region at low frequency. The decrease in the gradient of the linear region was indicative of Li ion diffusion occurring within the active material.[62] The diameter of the semi-circle at median frequency indicated the resistance of the newly formed SEI layer (R_{SEI}).[63] Figure 6(b) shows that among the four types of electrode, the total resistance ($R_s + R_{CT} + R_{SEI}$) was reduced the most for the [Top C] electrode, from ~1300 to ~500 Ω cm^2.

Figure 6(c) shows a Nyquist plot of the four types of electrode after one lithiation and delithiation cycle. The two semi-circles start to overlap, similar to other Si-based anodes, indicative of partial SEI breakdown during delithiation.[60] The total resistance ($R_s + R_{CT} + R_{SEI}$) was reduced further to ~300 Ω cm^2 for the [Top C] and [Sandwich] electrodes, lower than 470 Ω cm^2 for the [Bottom C] electrode and 1050 Ω cm^2 for the [Blended] electrode. Note that the [Blended] electrode exhibited the lowest capacity and highest total resistance.

Figure 6(d) shows a Nyquist plot of the same four types of electrode after the 5th cycle lithiation while Figure 6(e) shows a Nyquist plot after the 5th cycle delithiation. The total resistance ($R_s + R_{CT} + R_{SEI}$) was 508 and 440 Ω cm^2 for the [Sandwich] and [Top C] electrodes respectively, lower than 705 and 990 Ω cm^2 for the [Bottom C] and [Blended] electrodes respectively in Figure 6(d). The total resistance ($R_s + R_{CT} + R_{SEI}$) was ~260 Ω cm^2 for both [Sandwich] and [Top C] electrodes, lower than 345 and 590 Ω cm^2 for the [Bottom C] and [Blended] electrodes respectively in Figure 6(e). The consistent lower total resistance ($R_s + R_{CT} + R_{SEI}$) for the [Top C] and [Sandwich] electrodes after the first cycle and the 5th cycles lithiation and delithiation indicated thinner and more stable SEI for the [Top C] and [Sandwich] electrodes than the [Bottom C] and [Blended] electrodes.[55] This is postulated to arise because the porous C layer at the interface between the Si/SiO_x layer and the separator ensures that the reactive Si/SiO_x layer is not directly against the separator where the Li ion concentration is highest and

there is a tendency for excessive expansion and damage to occurs. Although some capacity must be sacrificed, electrode stability is improved because fracture of the Si/SiO_x particles is less likely, as shown by the improved cycling performance in Figure 5(d), which is further investigated in the following section.

The lower R_{CT} for the as-sprayed [Sandwich] and [Bottom C] electrodes indicated that the C layer on the current collector increased electronic connectivity at the otherwise relatively resistive interface between the current collector and the electrode, so that a higher proportion of potentially active Si/SiO_x was electrically connected and thus able to contribute to the electrochemical storage of Li ions,[29, 40] consistent with the higher capacities and rate capabilities of the [Sandwich] and [Bottom C] electrodes in Figures 5(a) and 5(d). The relatively high mechanical compliance and sponge-like microstructure of the C layer allowed electrical contact to be maintained, even when the Si/SiO_x active material expanded and contracted during lithiation and delithiation. This buffering of the insertion strain of the Si/SiO_x active material prevented a loss of mechanical and electrical integrity of the electrode as a whole, ensuring electrical contact was maintained.

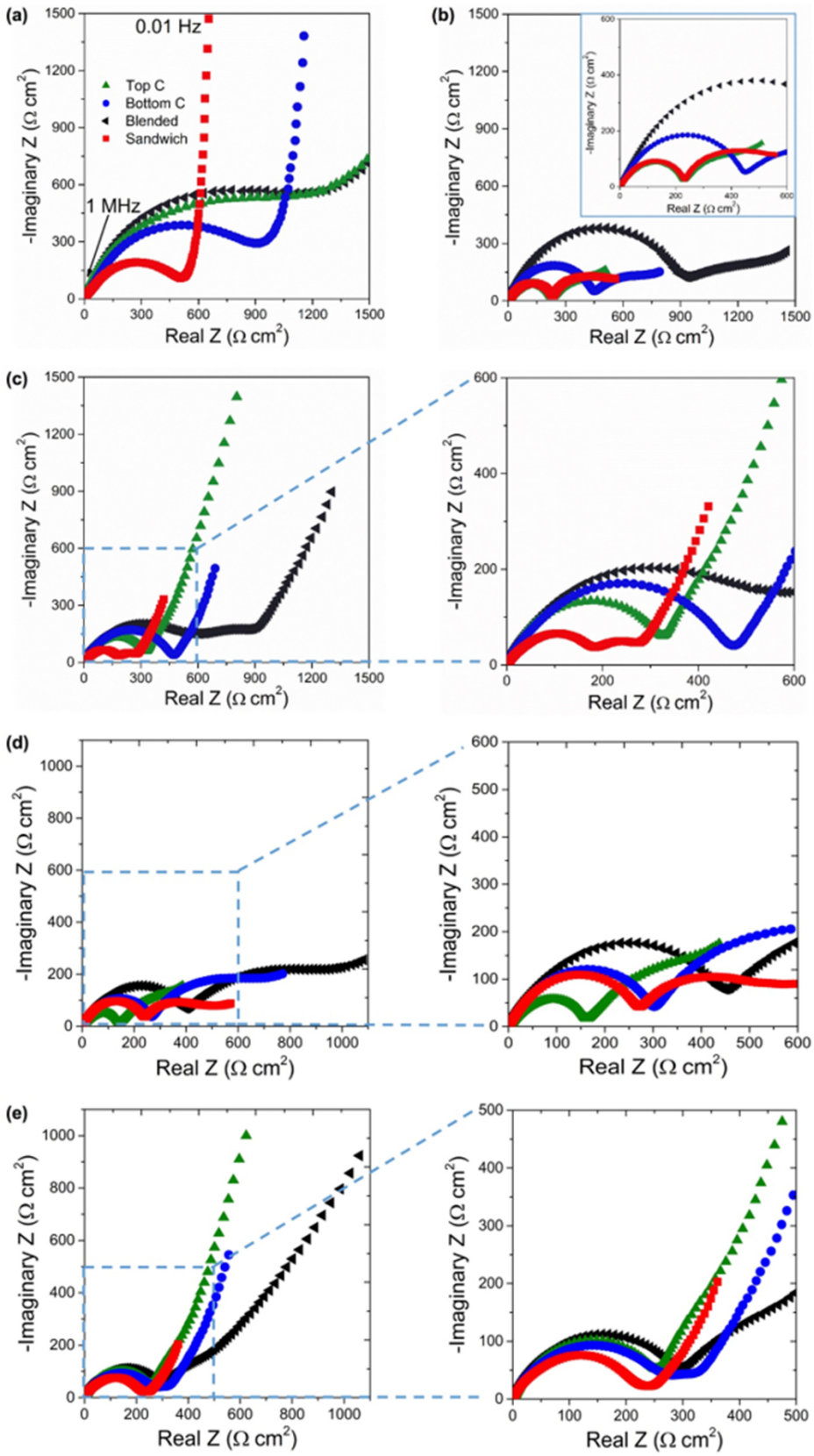
(a)
0.01 Hz
1 MHz
Top C
Bottom C
Blended
Sandwich
-Imaginary Z (Ω cm²)
Real Z (Ω cm²)
(b)
(c)
(d)
(e)

Figure 6. EIS measurements of the four types of electrode in the conditions of (a) as-sprayed; (b) after first lithiation; (c) after one lithiation and delithiation cycle; (d) at the 5th lithiation state; and (e) at the 5th delithiation state.

3.4 Post-cycle electrode structure

Figure 7 is cross-sectional SEM images of the four types of electrode after the first lithiation and delithiation cycle at 50 mA g^{-1} showing a through thickness net expansion of 27% averaged across all electrodes. All the electrodes were qualitatively denser than the as-sprayed electrodes, and for the layered electrodes, both Si/SiO$_x$ and C layers showed consolidation *i.e.* expansion/contraction and buffering of strain occurred in both layers but was not fully reversible. There was delamination of the electrode from the current collector for the [Blended] electrode (~1 µm gap at the interface between the current collector and the electrode), perhaps suggesting that the randomly distributed C nanoparticles in the [Blended] electrode could not buffer the strain caused by the expansion of Si/SiO$_x$ as effectively as the discrete C layers in the other electrodes, but many more cross-sections would be required to be certain this was reproducible.

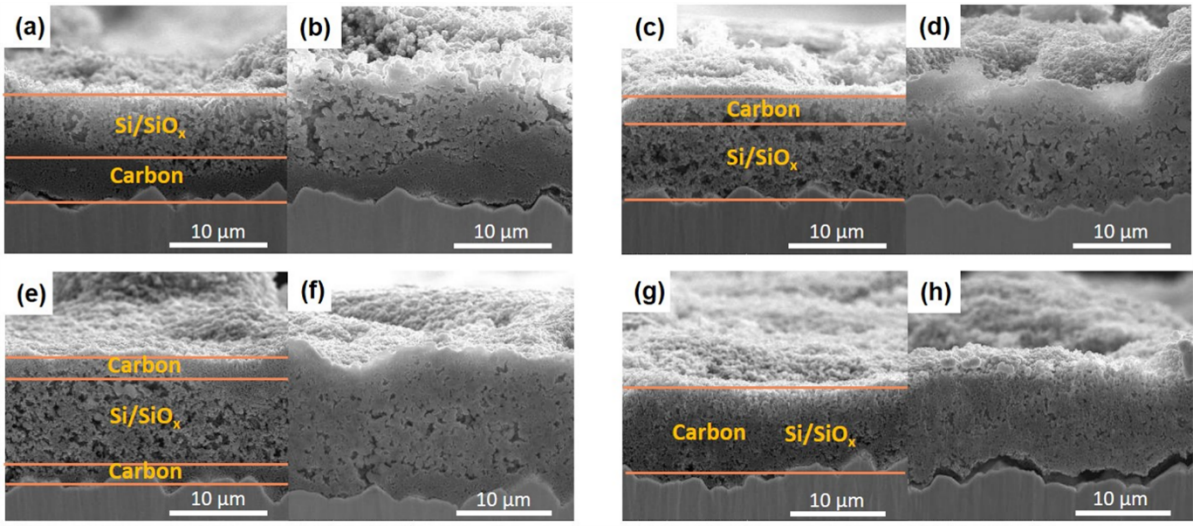

Figure 7. Cross-sectional SEM images of the [Bottom C] electrode (a) before and (b) after; [Top C] electrode (c) before and (d) after; [Sandwich] electrode (e) before and (f) after; [Blended] electrode (g) before and (h) after one charge and discharge cycle at 50 mA g^{-1}.

Figure 8 shows cross-sectional SEM images of the four types of electrode after 100 cycles, showing further expansion and porosity reduction in all regions of all electrodes. There were now extensive cracks and delamination in the [Bottom C] and [Blended] electrodes, because even small spatial inhomogeneities in Si/SiO_x expansion will have caused different levels of local strain and some lateral displacement that promoted local cracking/rearrangement. These cracks and material rearrangements in the [Bottom C] and [Blended] electrodes exposed active Si/SiO_x surfaces for further formation of SEI and consumption of Li ions.[29] The large fractures eventually led to disintegration of the [Bottom C] and [Blended] electrodes.

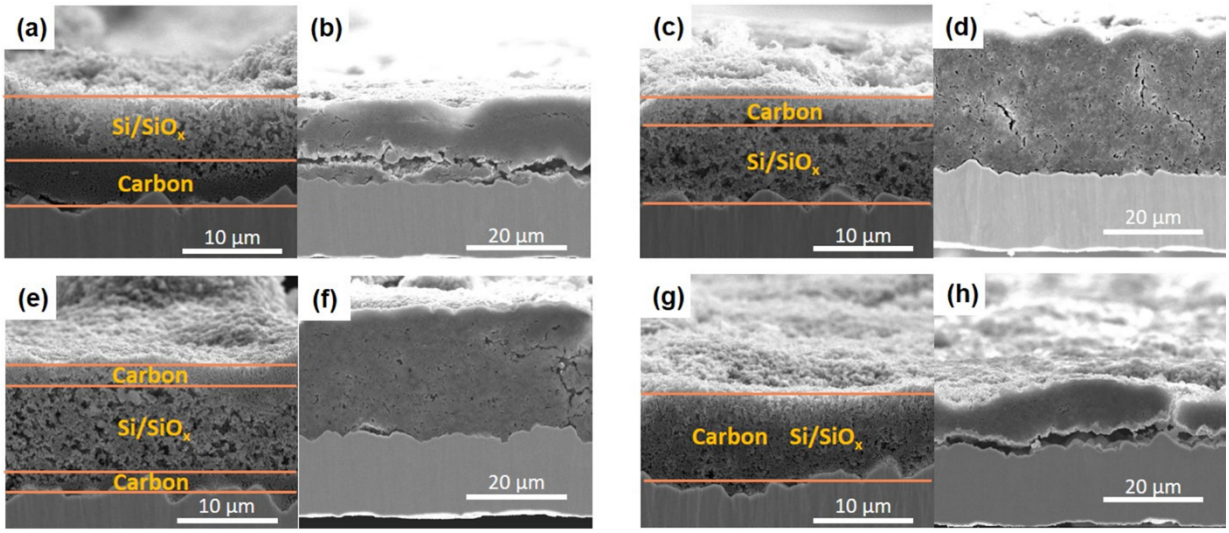

Figure 8. Cross-sectional SEM images of the [Bottom C] electrode (a) before and (b) after; [Top C] electrode (c) before and (d) after; [Sandwich] electrode (e) before and (f) after; [Blended] electrode (g) before and (h) after 100 charge and discharge cycles at 50 mA g^{-1}.

In contrast, the integrity of the [Top C] and [Sandwich] electrodes was preserved, even after 100 cycles, albeit with a lower initial capacity for the [Top C] electrode. The cycling performance in Figure 5(d), the EIS measurements in Figure 6, and the post-cycle cross-sectional SEM images in Figures 7 and 8 all suggest that the beneficial role of the C layer at the interface between the separator and the Si/SiO_x layer may be to "shield" the reactive Si/SiO_x layer from the highest concentrations of Li ions, which will always be at the separator (especially in these half-cell arrangements *versus* Li foil).[64] Here, the role of the C layer next to the separator is not so much to buffer the mechanical strain directly (although

that may still be helpful) but to buffer the Li ion concentrations and to avoid very high local Li concentrations that lead to severe swelling, pulverisation and loss of electrical connectivity and capacity.

4. Conclusions

A new multi-scale approach to buffering the strain in high capacity Si-based anodes has been developed, using arrangements and mixtures of materials at both the nano- and micro-scale. The nanostructure and electrode microstructure were investigated to identify optimum capacity, rate capability and cycling stability of Si-based anodes for Li ion batteries. A Si/SiO_x nanocomposite of Si nanocrystals embedded in amorphous SiO_x nanospheres was synthesised where the SiO_x phase accommodated volume expansion of the Si phase at the nano-scale. Four types of electrode structure were then layer-by-layer assembled with the intention that C nanoparticle layers would buffer the expansion/contraction strains of the Si/SiO_x layer at a larger scale. Additionally, a C layer at the interface between the current collector and the Si/SiO_x layer improved capacity and rate capability through reduced electrical interfacial resistance, while the C layer at the interface between the separator and the Si/SiO_x layer improved cycling stability primarily by shielding the Si/SiO_x layer from the very highest Li ion concentrations directly adjacent to the separator that can lead to extreme expansion and failure on lithiation. We suggest that while this approach is demonstrated for the Si/SiO_x system, the ideas could be extended to other high-capacity alloy-type electrode materials that similarly suffer from large volume changes during cycling such as Sn-, Ge- based materials for Li rechargeable batteries, and other systems such as Li-air, Li-S and Na-ion batteries where electrode-scale microstructural design has yet to be explored using scalable fabrication techniques.

Conflicts of interest

There are no conflicts of interest to declare.

Acknowledgements

This work was partly supported by the UK Engineering and Physical Research Council through Grant EP/M009521/1 – "Enabling Next Generation Li-ion Batteries", and partly supported by Basic Research Program through the National Research Foundation of Korea (NRF) grant funded by the Korean government (MSIT) (NRF-2017R1A2B2012847).

References

1. Armand, M.; Tarascon, J.-M., Building Better Batteries. *Nature* **2008,** *451*, 652-657.
2. Kohs, W.; Santner, H. J.; Hofer, F.; Schröttner, H.; Doninger, J.; Barsukov, I.; Buqa, H.; Albering, J. H.; Möller, K. C.; Besenhard, J. O.; Winter, M., A Study on Electrolyte Interactions with Graphite Anodes Exhibiting Structures with Various Amounts of Rhombohedral Phase. *Journal of Power Sources* **2003,** *119*, 528-537.
3. Besenhard, J.; Yang, J.; Winter, M., Will Advanced Lithium-Alloy Anodes Have a Chance in Lithium-Ion Batteries? *Journal of Power Sources* **1997,** *68*, 87-90.
4. Obrovac, M.; Chevrier, V., Alloy Negative Electrodes for Li-Ion Batteries. *Chemical Reviews* **2014,** *114*, 11444-11502.
5. Zhang, W.-J., A Review of the Electrochemical Performance of Alloy Anodes for Lithium-Ion Batteries. *Journal of Power Sources* **2011,** *196*, 13-24.
6. Kim, H.; Seo, M.; Park, M. H.; Cho, J., A Critical Size of Silicon Nano-Anodes for Lithium Rechargeable Batteries. *Angewandte Chemie International Edition* **2010,** *49*, 2146-2149.
7. Park, E.; Park, M. S.; Lee, J.; Kim, K. J.; Jeong, G.; Kim, J. H.; Kim, Y. J.; Kim, H., A Highly Resilient Mesoporous SiO_x Lithium Storage Material Engineered by Oil-Water Templating. *ChemSusChem* **2015,** *8*, 688-694.
8. Park, E.; Yoo, H.; Lee, J.; Park, M.-S.; Kim, Y.-J.; Kim, H., Dual-Size Silicon Nanocrystal-Embedded SiO_X Nanocomposite as a High-Capacity Lithium Storage Material. *ACS Nano* **2015,** *9*, 7690-7696.
9. Park, E.; Kim, J.; Chung, D. J.; Park, M. S.; Kim, H.; Kim, J. H., Si/SiO_x-Conductive Polymer Core-Shell Nanospheres with an Improved Conducting Path Preservation for Lithium-Ion Battery. *ChemSusChem* **2016,** *9*, 2754-2758.
10. Bae, J.; Kim, D. S.; Yoo, H.; Park, E.; Lim, Y.-G.; Park, M.-S.; Kim, Y.-J.; Kim, H., High-Performance Si/SiO_X Nanosphere Anode Material by Multipurpose Interfacial Engineering with Black TiO_{2-X}. *ACS Applied Materials & Interfaces* **2016,** *8*, 4541-4547.
11. Yu, B.-C.; Hwa, Y.; Kim, J.-H.; Sohn, H.-J., A New Approach to Synthesis of Porous SiO_X Anode for Li-Ion Batteries Via Chemical Etching of Si Crystallites. *Electrochimica Acta* **2014,** *117*, 426-430.
12. Zhang, J.; Zhang, C.; Liu, Z.; Zheng, J.; Zuo, Y.; Xue, C.; Li, C.; Cheng, B., High-Performance Ball-Milled SiO_X Anodes for Lithium Ion Batteries. *Journal of Power Sources* **2017,** *339*, 86-92.
13. Yoo, S.; Lee, J. I.; Shin, M.; Park, S., Large-Scale Synthesis of Interconnected Si/SiO_x Nanowire Anodes for Rechargeable Lithium-Ion Batteries. *ChemSusChem* **2013,** *6*, 1153-1157.
14. Yang, J.; Takeda, Y.; Imanishi, N.; Capiglia, C.; Xie, J.; Yamamoto, O., SiO_X-Based Anodes for Secondary Lithium Batteries. *Solid State Ionics* **2002,** *152*, 125-129.
15. Cui, L.-F.; Ruffo, R.; Chan, C. K.; Peng, H.; Cui, Y., Crystalline-Amorphous Core-Shell Silicon Nanowires for High Capacity and High Current Battery Electrodes. *Nano Letters* **2008,** *9*, 491-495.
16. Yao, Y.; McDowell, M. T.; Ryu, I.; Wu, H.; Liu, N.; Hu, L.; Nix, W. D.; Cui, Y., Interconnected Silicon Hollow Nanospheres for Lithium-Ion Battery Anodes with Long Cycle Life. *Nano Letters* **2011,** *11*, 2949-2954.

17. Park, M.-H.; Kim, M. G.; Joo, J.; Kim, K.; Kim, J.; Ahn, S.; Cui, Y.; Cho, J., Silicon Nanotube Battery Anodes. *Nano Letters* **2009,** *9*, 3844-3847.
18. Li, X.; Meduri, P.; Chen, X.; Qi, W.; Engelhard, M. H.; Xu, W.; Ding, F.; Xiao, J.; Wang, W.; Wang, C., Hollow Core-Shell Structured Porous Si-C Nanocomposites for Li-Ion Battery Anodes. *Journal of Materials Chemistry* **2012,** *22*, 11014-11017.
19. Yoo, J. K.; Kim, J.; Jung, Y. S.; Kang, K., Scalable Fabrication of Silicon Nanotubes and Their Application to Energy Storage. *Advanced Materials* **2012,** *24*, 5452-5456.
20. Wu, H.; Chan, G.; Choi, J. W.; Ryu, I.; Yao, Y.; McDowell, M. T.; Lee, S. W.; Jackson, A.; Yang, Y.; Hu, L., Stable Cycling of Double-Walled Silicon Nanotube Battery Anodes through Solid-Electrolyte Interphase Control. *Nature Nanotechnology* **2012,** *7*, 310-315.
21. Liu, N.; Lu, Z.; Zhao, J.; McDowell, M. T.; Lee, H.-W.; Zhao, W.; Cui, Y., A Pomegranate-Inspired Nano-scale Design for Large-Volume-Change Lithium Battery Anodes. *Nature Nanotechnology* **2014,** *9*, 187-192.
22. Zhao, X.; Sánchez, B. M.; Dobson, P. J.; Grant, P. S., The Role of Nanomaterials in Redox-Based Supercapacitors for Next Generation Energy Storage Devices. *Nanoscale* **2011,** *3*, 839-855.
23. Liu, N.; Wu, H.; McDowell, M. T.; Yao, Y.; Wang, C.; Cui, Y., A Yolk-Shell Design for Stabilized and Scalable Li-Ion Battery Alloy Anodes. *Nano letters* **2012,** *12*, 3315-3321.
24. Luo, L.; Yang, H.; Yan, P.; Travis, J. J.; Lee, Y.; Liu, N.; Molina Piper, D.; Lee, S.-H.; Zhao, P.; George, S. M., Surface-Coating Regulated Lithiation Kinetics and Degradation in Silicon Nanowires for Lithium Ion Battery. *ACS nano* **2015,** *9*, 5559-5566.
25. Ng, S. H.; Wang, J.; Wexler, D.; Konstantinov, K.; Guo, Z. P.; Liu, H. K., Highly Reversible Lithium Storage in Spheroidal Carbon-Coated Silicon Nanocomposites as Anodes for Lithium-Ion Batteries. *Angewandte Chemie International Edition* **2006,** *45*, 6896-6899.
26. Fyta, M. G.; Remediakis, I. N.; Kelires, P. C.; Papaconstantopoulos, D. A., Insights into the Fracture Mechanisms and Strength of Amorphous and Nanocomposite Carbon. *Physical review letters* **2006,** *96*, 185503.
27. Li, W.; Cao, K.; Wang, H.; Liu, J.; Zhou, L.; Yao, H., Carbon Coating May Expedite the Fracture of Carbon-Coated Silicon Core-Shell Nanoparticles During Lithiation. *Nanoscale* **2016,** *8*, 5254-5259.
28. Yi, R.; Dai, F.; Gordin, M. L.; Chen, S.; Wang, D., Micro-Sized Si-C Composite with Interconnected Nanoscale Building Blocks as High-Performance Anodes for Practical Application in Lithium-Ion Batteries. *Advanced Energy Materials* **2013,** *3*, 295-300.
29. Reyes Jimenez, A.; Klopsch, R.; Wagner, R.; Rodehorst, U. C.; Kolek, M.; Nolle, R.; Winter, M.; Placke, T., A Step toward High-Energy Silicon-Based Thin Film Lithium Ion Batteries. *ACS Nano* **2017,** *11*, 4731-4744.
30. Kraytsberg, A.; Ein-Eli, Y., Conveying Advanced Li-Ion Battery Materials into Practice The Impact of Electrode Slurry Preparation Skills. *Advanced Energy Materials* **2016,** *6*, 1600655.
31. Dai, Y.; Srinivasan, V., On Graded Electrode Porosity as a Design Tool for Improving the Energy Density of Batteries. *Journal of The Electrochemical Society* **2016,** *163*, A406-A416.
32. Liu, L.; Guan, P.; Liu, C., Experimental and Simulation Investigations of Porosity Graded Cathodes in Mitigating Battery Degradation of High Voltage Lithium-Ion Batteries. *Journal of The Electrochemical Society* **2017,** *164*, A3163-A3173.
33. Qi, Y.; Jang, T.; Ramadesigan, V.; Schwartz, D. T.; Subramanian, V. R., Is There a Benefit in Employing Graded Electrodes for Lithium-Ion Batteries? *Journal of The Electrochemical Society* **2017,** *164*, A3196-A3207.
34. Du, W.; Xue, N.; Sastry, A. M.; Martins, J. R.; Shyy, W., Energy Density Comparison of Li-Ion Cathode Materials Using Dimensional Analysis. *Journal of the Electrochemical society* **2013,** *160*, A1187-A1193.
35. Huang, C.; Young, N. P.; Zhang, J.; Snaith, H. J.; Grant, P. S., A Two Layer Electrode Structure for Improved Li Ion Diffusion and Volumetric Capacity in Li Ion Batteries. *Nano Energy* **2017,** *31*, 377-385.

36. Park, M.-S.; Park, E.; Lee, J.; Jeong, G.; Kim, K. J.; Kim, J. H.; Kim, Y.-J.; Kim, H., Hydrogen Silsequioxane-Derived Si/SiO_X Nanospheres for High-Capacity Lithium Storage Materials. *ACS Applied Materials & Interfaces* **2014,** *6*, 9608-9613.
37. Pauthe, M.; Bernstein, E.; Dumas, J.; Saviot, L.; Pradel, A.; Ribes, M., Preparation and Characterisation of Si Nanocrystallites Embedded in a Silica Matrix. *Journal of Materials Chemistry* **1999,** *9*, 187-191.
38. Soraru, G. D.; Modena, S.; Bettotti, P.; Das, G.; Mariotto, G.; Pavesi, L., Si Nanocrystals Obtained through Polymer Pyrolysis. *Applied physics letters* **2003,** *83*, 749-751.
39. Huang, C.; Zhang, J.; Snaith, H. J.; Grant, P. S., Engineering the Membrane/Electrode Interface to Improve the Performance of Solid-State Supercapacitors. *ACS Applied Materials & Interfaces* **2016,** *8*, 20756-20765.
40. Huang, C.; Zhang, J.; Young, N. P.; Snaith, H. J.; Grant, P. S., Solid-State Supercapacitors with Rationally Designed Heterogeneous Electrodes Fabricated by Large Area Spray Processing for Wearable Energy Storage Applications. *Scientific Reports* **2016,** *6*, 25684.
41. Marks, T.; Trussler, S.; Smith, A.; Xiong, D.; Dahn, J., A Guide to Li-Ion Coin-Cell Electrode Making for Academic Researchers. *Journal of The Electrochemical Society* **2011,** *158*, A51-A57.
42. Tao, H.-C.; Huang, M.; Fan, L.-Z.; Qu, X., Interweaved Si@SiO_x/C Nanoporous Spheres as Anode Materials for Li-Ion Batteries. *Solid State Ionics* **2012,** *220*, 1-6.
43. Zhang, T.; Gao, J.; Zhang, H.; Yang, L.; Wu, Y.; Wu, H., Preparation and Electrochemical Properties of Core-Shell Si/SiO Nanocomposite as Anode Material for Lithium Ion Batteries. *Electrochemistry Communications* **2007,** *9*, 886-890.
44. Hu, Y. S.; Demir-Cakan, R.; Titirici, M. M.; Müller, J. O.; Schlögl, R.; Antonietti, M.; Maier, J., Superior Storage Performance of a Si@ SiO_x/C Nanocomposite as Anode Material for Lithium-Ion Batteries. *Angewandte Chemie International Edition* **2008,** *47*, 1645-1649.
45. Qiang, W.; Huanhuan, H.; Jian, W.; Zhurui, S., Fabrication of SiO_x Ultra-Fine Nanoparticles by Ir Nanosecond Laser Ablation as Anode Materials for Lithium Ion Battery. *Applied Surface Science* **2017,** *422*, 155-161.
46. Elia, G. A.; Hassoun, J., A SiO_x-Based Anode in a High-Voltage Lithium-Ion Battery. *ChemElectroChem* **2017,** *4*, 2164-2168.
47. Xu, Q.; Sun, J. K.; Yin, Y. X.; Guo, Y. G., Facile Synthesis of Blocky SiO_x/C with Graphite-Like Structure for High-Performance Lithium-Ion Battery Anodes. *Advanced Functional Materials* **2018,** *28*, 1705235.
48. Zhang, Q.; Lin, N.; Xu, T.; Shen, K.; Li, T.; Han, Y.; Zhou, J.; Qian, Y., Scalable Synthesis of Carbon Stabilized SiO/Graphite Sheets Composite as Anode for High-Performance Li Ion Batteries. *RSC Advances* **2017,** *7*, 39762-39766.
49. Miyazaki, R.; Ohta, N.; Ohnishi, T.; Takada, K., Anode Properties of Silicon-Rich Amorphous Silicon Suboxide Films in All-Solid-State Lithium Batteries. *Journal of Power Sources* **2016,** *329*, 41-49.
50. Homma, K.; Kambara, M.; Yoshida, T., High Throughput Production of Nanocomposite SiO_X Powders by Plasma Spray Physical Vapor Deposition for Negative Electrode of Lithium Ion Batteries. *Science and technology of advanced materials* **2014,** *15*, 025006.
51. Yang, J.; Takeda, Y.; Imanishi, N.; Capiglia, C.; Xie, J.; Yamamoto, O., SiO_x-Based Anodes for Secondary Lithium Batteries. *Solid State Ionics* **2002,** *152*, 125-129.
52. Lee, J.; Koo, J.; Jang, B.; Kim, S., Quantitative Relationships between Microstructures and Electrochemical Properties in Si Core-SiO_X Shell Nanoparticles for Li-Ion Battery Anodes. *Journal of Power Sources* **2016,** *329*, 79-87.
53. Qian, L.; Lan, J.-L.; Xue, M.; Yu, Y.; Yang, X., Two-Step Ball-Milling Synthesis of a Si/SiO_X/C Composite Electrode for Lithium Ion Batteries with Excellent Long-Term Cycling Stability. *RSC Advances* **2017,** *7*, 36697-36704.
54. Si, Q.; Hanai, K.; Ichikawa, T.; Phillipps, M.; Hirano, A.; Imanishi, N.; Yamamoto, O.; Takeda, Y., Improvement of Cyclic Behavior of a Ball-Milled SiO and Carbon Nanofiber Composite Anode for Lithium-Ion Batteries. *Journal of Power Sources* **2011,** *196*, 9774-9779.

55. Zhang, L.; Deng, J.; Liu, L.; Si, W.; Oswald, S.; Xi, L.; Kundu, M.; Ma, G.; Gemming, T.; Baunack, S., Hierarchically Designed SiO_x/SiO_y Bilayer Nanomembranes as Stable Anodes for Lithium Ion Batteries. *Advanced Materials* **2014,** *26*, 4527-4532.
56. Lee, S. J.; Kim, H. J.; Hwang, T. H.; Choi, S.; Park, S. H.; Deniz, E.; Jung, D. S.; Choi, J. W., Delicate Structural Control of Si-SiO_X-C Composite Via High-Speed Spray Pyrolysis for Li-Ion Battery Anodes. *Nano letters* **2017,** *17*, 1870-1876.
57. Gao, C.; Zhao, H.; Lv, P.; Wang, C.; Wang, J.; Zhang, T.; Xia, Q., Superior Cycling Performance of SiO_x/C Composite with Arrayed Mesoporous Architecture as Anode Material for Lithium-Ion Batteries. *Journal of The Electrochemical Society* **2015,** *161*, A2216-A2221.
58. Liu, W.-R.; Yen, Y.-C.; Wu, H.-C.; Winter, M.; Wu, N.-L., Nano-Porous SiO/Carbon Composite Anode for Lithium-Ion Batteries. *Journal of applied electrochemistry* **2009,** *39*, 1643-1649.
59. Wang, J.; Zhao, H.; He, J.; Wang, C.; Wang, J., Nano-Sized SiO_X/C Composite Anode for Lithium Ion Batteries. *Journal of Power Sources* **2011,** *196*, 4811-4815.
60. Kim, G.-T.; Kennedy, T.; Brandon, M.; Geaney, H.; Ryan, K. M.; Passerini, S.; Appetecchi, G. B., Behavior of Germanium and Silicon Nanowire Anodes with Ionic Liquid Electrolytes. *ACS nano* **2017,** *11*, 5933-5943.
61. Zhang, Y.; Pan, Y.; Chen, Y.; Lucht, B. L.; Bose, A., Towards Reducing Carbon Content in Silicon/Carbon Anodes for Lithium Ion Batteries. *Carbon* **2017,** *112*, 72-78.
62. Ruffo, R.; Hong, S. S.; Chan, C. K.; Huggins, R. A.; Cui, Y., Impedance Analysis of Silicon Nanowire Lithium Ion Battery Anodes. *The Journal of Physical Chemistry C* **2009,** *113*, 11390-11398.
63. Chakrapani, V.; Rusli, F.; Filler, M. A.; Kohl, P. A., Quaternary Ammonium Ionic Liquid Electrolyte for a Silicon Nanowire-Based Lithium Ion Battery. *The Journal of Physical Chemistry C* **2011,** *115*, 22048-22053.
64. Park, J. H.; Ku, J.; Lim, J. W.; Choi, J.-m.; Son, I. H., Adhesive Interlayer between Active Film and Current Collector for Improving the Performance of Silicon Anodes of Li-Ion Batteries. *Journal of Electroanalytical Chemistry* **2016,** *778*, 53-56.

Table of contents

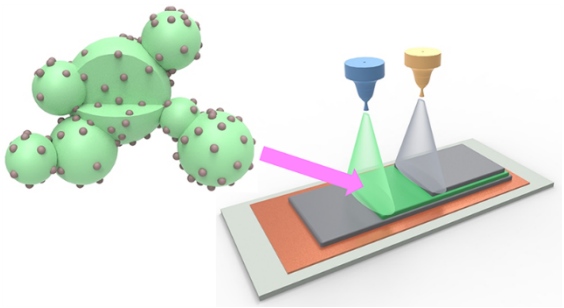

Combining micro-structuring of electrode architecture with nano-engineering of material improved multiple performance metrics of Si/SiO_x anodes using scalable spray deposition.